Thermal Modeling of Disordered Materials

Jason M. Larkin

August 2013

School of Computer Science
Carnegie Mellon University
Pittsburgh, PA 15213

Thesis Committee:
Alan J. H. McGaughey, Chair
Jonathan Malen
Craig Maloney
Michael Widom

*Submitted in partial fulfillment of the requirements
for the degree of Doctor of Philosophy.*

For my dog

Abstract

A short summary.

Acknowledgments

test

Contents

List of Figures

List of Tables

Chapter 1

Introduction

There are two sections to this introductory chapter.

Chapter 2

Predicting properties of alloys

There are two sections to this introductory chapter.

Chapter 3

Vibrational Mean Free Paths in Amorphous Materials

There are two sections to this introductory chapter.

Chapter 4

Origin of the Exceptionally-Low Thermal Conductivity of Fullerene-Derived PCBM thin films

There are two sections to this introductory chapter.

Chapter 5

Conclusion

There are two sections to this introductory chapter.

Appendix A

Vibrational Lifetimes from Molecular Dynamics

Two frequency-domain methods for predicting phonon frequencies and lifetimes using the phonon spectral energy density are described. Both methods draw input from molecular dynamics simulations and lattice dynamics calculations, but differ in the form of the phonon spectral energy density. One phonon spectral energy density expression (referred to as Φ) can be formally derived from lattice dynamics theory. A similar approach in the time domain has been validated [Turney et al. *Phys. Rev. B* **79**, 224305 (2009)]. The other phonon spectral energy density expression (referred to as Φ') has been proposed [Thomas et al., *Phys. Rev. B* **81**, 081411(R) (2010)] but not validated. The expressions for Φ and Φ' are presented and then applied to predict the phonon properties and thermal conductivities of three systems: Lennard-Jones argon, Stillinger-Weber silicon, and a carbon nanotube modeled using the Reactive Empirical Bond Order potential. Φ' does not capture the total phonon spectral energy density predicted by Φ and therefore cannot correctly predict the phonon lifetimes or thermal conductivity. Its use infuture work is discouraged and we reccomend the use of Φ.

A.1   Introduction

Phonons are the dominant carriers of thermal energy in dielectric and semiconducting crystals [3, 4, 5, 6, 7**?**]. While substantial effort has been devoted to developing theories of phonon transport, the current understanding is incomplete, even in bulk materials. For example, which phonon modes dominate thermal energy transport and the importance of interactions involving four or more phonons are still being investigated [3, 5, 6, 8, 9]. The situation becomes more complicated in nanostructures, where the phonons also interact with free surfaces and interfaces [2, 10, 11, 12, 13, 14, 15, 16, 17, 18, 19, 20**?**].

Analytical models of thermal transport, such as the Debye model, are limited by the necessary approximations and assumptions [21, 22, 23]. With the Green-Kubo or non-equilibrium direct methods, molecular dynamics (MD) simulations can be used to predict thermal conductivity, but only in a classical (i.e., high-temperature) framework [1, 9, 17, 24, 25, 26, 27]. Because the analysis in these two MD-based methods is performed at the system level, no information about

the phonons is obtained. Phonon specific heats, group velocities, and lifetimes are the required inputs for predicting thermal conductivity at the phonon-mode-level using Boltzmann transport equation-based models [1, 2, 9, 23, 24, 25, 27]. These phonon properties can be predicted using harmonic and anharmonic lattice dynamics calculations [1, 6, 7, 24, 28**?**], where quantum statistical effects can be naturally included. Anharmonic lattice dynamics calculations are limited to three-phonon scattering events, however, and are thus only valid at low temperatures [1, 5, 6, 9].

At high temperature, four-phonon and higher-order processes become important to thermal transport [1, 5, 6, 9]. All orders of phonon processes are present in a MD simulation as the positions and momenta of the atoms are evolved using the full anharmonicity of the interatomic interactions [9, 25]. Phonon properties can be predicted from a MD simulation using normal mode analysis in the time domain [1, 2, 24, 25, 29, 30]. In Section A.2.1, we will describe how this approach can be performed in the frequency-domain using the phonon spectral energy density (SED, referred to as Φ). An alternative expression for the phonon SED (referred to as Φ'), was recently proposed but has not been rigorously tested [31, 32, 33]. Φ' was first used to predict the phonon dispersion curves of carbon nanotubes (CNTs) [31]. Thomas et al. used Φ' to predict the phonon lifetimes and thermal conductivity of isolated and water-filled CNTs, obtaining good agreement with other atomistic predictions [33]. The phonon lifetime reductions speculated for water-filled CNTs [33] and CNTs on SiO_2 substrates [34] suggest that Φ' captures phonon physics at least qualitatively. The phonon lifetimes and thermal conductivity for PbTe [35] and Half Heusler alloys [36] have also been predicted using Φ'. De Koker predicted the phonon lifetimes and thermal conductivity for MgO using an expression similar to Φ' (but different than Φ) [**?**]. Another recent atomistic study using Stillinger-Weber silicon predicted phonon lifetimes using both Φ and Φ', but a detailed comparison of the predictions between the two was not performed [37].

The objective of this work is to assess the validity of Φ' as a phonon SED by comparing the phonon properties it predicts to those predicted by Φ. In Section A.2.1, we present the correct phonon SED (Φ), which requires the phonon mode eigenvectors. The expression for Φ is well-defined theoretically and has been tested and validated in previous studies in the time domain [1, 24]. In Section A.2.2, we present the proposed alternative expression for the phonon SED, Φ', which does not require the phonon mode eigenvector [33]. Phonon frequencies, lifetimes, and thermal conductivities are then predicted and compared using Φ and Φ' for three test systems: Lennard-Jones (LJ) argon [38] in Section A.4.1, Stillinger-Weber (SW) silicon [39] in Section A.4.2, and an (8,8) CNT modeled with the reactive empirical bond order (REBO) potential [**?**] in Section A.4.3. While Φ' is found to accurately predict the phonon frequencies, we find that it does not correctly predict the phonon lifetimes because it does not capture the total phonon spectral energy density.

A.2   Phonon Spectral Energy Density

A.2.1   As Derived from Normal Mode Coordinates, Φ

The correct expression for the phonon SED, Φ, can be derived from the formulation of anharmonic lattice dynamics theory [5, 6, 7 ?]. As shown in Appendix (REF), the phonon SED at wavevector $\boldsymbol{\kappa}$ is a function of frequency, ω, and is given by

$$\Phi(\boldsymbol{\kappa}, \omega) = \sum_{\nu}^{3n} C_0(^{\boldsymbol{\kappa}}_{\nu}) \frac{\Gamma(^{\boldsymbol{\kappa}}_{\nu})/\pi}{[\omega_0(^{\boldsymbol{\kappa}}_{\nu}) - \omega]^2 + \Gamma^2(^{\boldsymbol{\kappa}}_{\nu})}, \tag{A.1}$$

which is a superposition of $3n$ Lorentzian functions with centers at $\omega_0(^{\boldsymbol{\kappa}}_{\nu})$ and linewidths $\Gamma(^{\boldsymbol{\kappa}}_{\nu})$ (one for each polarization, ν). The $C_0(^{\boldsymbol{\kappa}}_{\nu})$ terms are mode-dependent constants. For simplicity, we refer to $\Phi(\boldsymbol{\kappa}, \omega)$ as Φ. The phonon kinetic energy normal mode coordinate, $\dot{q}(^{\boldsymbol{\kappa}}_{\nu}; t)$, is [7]

$$\dot{q}(^{\boldsymbol{\kappa}}_{\nu}; t) = 00 \sum_{\alpha,b,l}^{3,n,N} 01 \sum_{\alpha,b}^{3,n} \sum_{\boldsymbol{\kappa},\nu}^{N,3n} \sqrt{\frac{m_b}{N}} \dot{u}_\alpha(^{l}_{b}; t) \, e^*(^{\boldsymbol{\kappa}}_{\nu}\,^{b}_{\alpha}) \exp[i\boldsymbol{\kappa} \cdot \mathbf{r}_0(^{lal}_{0b0})], \tag{A.2}$$

where $e(^{\boldsymbol{\kappa}}_{\nu}\,^{b}_{\alpha})$ are the components of the time-independent phonon mode eigenvector (see Section A.3.2), n is the number of atoms in the unit cell, m_b is the mass of the bth atom in the unit cell and $\mathbf{r}_0(^{lal}_{0b0})$ is the equilibrium position vector of the lth unit cell. There are N total unit cells and $\dot{u}_\alpha(^{l}_{b}; t)$ is the α-component of the velocity of the bth atom in the lth unit cell at time t.

Given a set of atomic velocities from MD simulation and the phonon mode eigenvector, Φ can be calculated using

$$\Phi(\boldsymbol{\kappa}, \omega) = 2 \sum_{\nu}^{3n} T(^{\boldsymbol{\kappa}}_{\nu}; \omega) = 2 \sum_{\nu}^{3n} \lim_{\tau_0 \to \infty} \frac{1}{2\tau_0} \left| \frac{1}{\sqrt{2\pi}} \int_0^{\tau_0} \dot{q}(^{\boldsymbol{\kappa}}_{\nu}; t) \exp(-i\omega t) dt \right|^2, \tag{A.3}$$

and then fit using Equation (A.18) to extract the phonon properties $\omega_0(^{\boldsymbol{\kappa}}_{\nu})$ and $\Gamma(^{\boldsymbol{\kappa}}_{\nu})$.

The phonon lifetime, $\tau(^{\boldsymbol{\kappa}}_{\nu})$, is defined as $1/[2\Gamma(^{\boldsymbol{\kappa}}_{\nu})]$. In practice, τ_0 should be much larger than the longest phonon lifetime and the continuous fourier transform in Equation (A.30) is performed using a discrete fast fourier transform (see Section A.4.1, A.4.2 and A.4.3).

Previous work using normal mode analysis has represented the phonon energy in the time domain [1, 2, 24, 25, 29, 30], while Φ is a representation of the phonon energy in the frequency domain. The time- and frequency-domain approaches are mathematically equivalent by use of the Wiener-Khinchin theorem [36, 40]. The frequency-domain approach has the advantage of predicting both the phonon lifetime and frequency by fitting a simpler function than is required in the time-domain approach.

A.2.2   Alternative Formulation, Φ'

We now seek to motivate the expression Φ' that was proposed in previous studies but has not been validated [31, 32, 33]. Thomas et al. [33] define

$$\Phi'(\boldsymbol{\kappa}, \omega) = \frac{1}{4\pi\tau_0} \sum_{\alpha}^{3} \sum_{b}^{n} \frac{m_b}{N} \left| \sum_{l}^{N} \int_0^{\tau_0} \dot{u}_\alpha(^{l}_{b}; t) \exp[\Theta] dt \right|^2, \tag{A.4}$$

13

where $\Theta \equiv i[\boldsymbol{\kappa} \cdot \mathbf{r}_0(\begin{smallmatrix}lal\\0b0\end{smallmatrix}) - \omega t]$. To understand this expression, we start with the real-space atomic velocities as represented by the normal mode velocities, $\dot{q}(\begin{smallmatrix}\boldsymbol{\kappa}'\\\nu\end{smallmatrix}; t)$ [7],

$$\dot{u}_\alpha(\begin{smallmatrix}l\\b\end{smallmatrix}; t) = 20 \sum_{\alpha,b,l}^{3,n,N} 21 \sum_{\alpha,b}^{3,n} \sum_{\boldsymbol{\kappa}',\nu}^{N,3n} \frac{1}{\sqrt{m_b N}} \exp\left[i\boldsymbol{\kappa}' \cdot \mathbf{r}_0(\begin{smallmatrix}lal\\0b0\end{smallmatrix})\right] e^*(\begin{smallmatrix}\boldsymbol{\kappa}' & b\\\nu & \alpha\end{smallmatrix}) \dot{q}(\begin{smallmatrix}\boldsymbol{\kappa}'\\\nu\end{smallmatrix}; t) . \tag{A.5}$$

Fourier transforming both sides of Equation (A.5) in time and space, taking the complex modulus, and summing over the atoms in the unit cell and the Cartesian directions yields

$$\lim_{\tau_0 \to \infty} \frac{1}{4\pi\tau_0} \sum_\alpha^3 \sum_b^n \frac{m_b}{N} \left| \sum_l^N \int_0^{\tau_0} \dot{u}_\alpha(\begin{smallmatrix}l\\b\end{smallmatrix}; t) \exp[\Theta] dt \right|^2 =$$

$$\lim_{\tau_0 \to \infty} \frac{1}{4\pi\tau_0} \sum_\alpha^3 \sum_b^n \left| \frac{m_b^{3/2}}{\sqrt{N}} \sum_l^N \sum_\nu^{3n} e^*(\begin{smallmatrix}\boldsymbol{\kappa} & b\\\nu & \alpha\end{smallmatrix}) \int_0^{\tau_0} \dot{q}(\begin{smallmatrix}\boldsymbol{\kappa}\\\nu\end{smallmatrix}; t) \exp[\Theta] dt \right|^2 , \tag{A.6}$$

where the the sum over $\boldsymbol{\kappa}'$ on the right-hand-side is reduced to a single wavevector by the orthogonality of the allowed wavevectors over the periodic domain. Equation (A.4) is the finite integration of the left-hand-side of Equation (A.6). For simplicity, we refer to $\Phi'(\boldsymbol{\kappa}, \omega)$ as Φ'. Given a set of atomic velocities, Thomas et al. extract the phonon properties $\omega_0(\begin{smallmatrix}\boldsymbol{\kappa}\\\nu\end{smallmatrix})$ and $\tau(\begin{smallmatrix}\boldsymbol{\kappa}\\\nu\end{smallmatrix})$ from Equation (A.4) by fitting Φ' for a given wavevector to a superposition of Lorentzian functions.

Thomas et al. [33] claim that Φ' represents the phonon SED. As seen in Equation (A.5), the phonon mode eigenvectors are necessary to properly map between the atomic velocities and the normal mode coordinates. This need for the eigenvectors is the essential difference between the expressions for Φ and Φ'. The potential advantage of Φ' is that other than the wavevectors, which can be determined from the crystal structure, no phonon properties need to be known *a priori*. However, to identify the degenerate modes in Φ', the phonon frequencies are necessary (see Section A.3.2). Since Φ' does not require the phonon mode eigenvector, it can (in principle) be used to study disordered systems or perturbed crystalline systems (e.g. dilute alloys [36], water-filled CNTs [33], and CNTs on substrates [34]). Despite its use in previous studies, Φ' has not been rigorously validated.

A.3 Computational Details

A.3.1 Allowed Wavevectors

Now that we have presented the two expressions for the phonon SED, we will provide the computational details of how they can be evaluated and used to predict phonon properties. The SED is defined for the allowed wavevectors of a crystal, which can be specified from the crystal structure's Bravais lattice, its basis (i.e., unit cell), and the size of the computational domain. A D-dimensional Bravais lattice is a collection of points with positions

$$\mathbf{r}_0(\begin{smallmatrix}lal\\0b0\end{smallmatrix}) = \sum_\alpha^D N_\alpha \mathbf{a}_\alpha, \tag{A.7}$$

14

where $\mathbf{a}_\alpha$ are the lattice vectors and N_α is an integer [7]. The unit cell is the building block of the crystal and is placed on the points defined by the Bravais lattice. The equilibrium position of any atom in the crystal can be described by

$$\mathbf{r}_0\left(\begin{smallmatrix}lal\\bbb\end{smallmatrix}\right) = \mathbf{r}_0\left(\begin{smallmatrix}lal\\0b0\end{smallmatrix}\right) + \mathbf{r}_0\left(\begin{smallmatrix}0a0\\bbb\end{smallmatrix}\right), \tag{A.8}$$

where $\mathbf{r}_0\left(\begin{smallmatrix}0a0\\bbb\end{smallmatrix}\right)$ is the equilibrium position of the bth atom in the unit cell relative to $\mathbf{r}_0\left(\begin{smallmatrix}lal\\0b0\end{smallmatrix}\right)$. The allowed wavevectors for any crystal structure are defined by

$$\boldsymbol{\kappa} = \sum_\alpha \mathbf{b}_\alpha \frac{n_\alpha}{N_\alpha}, \tag{A.9}$$

where $\mathbf{b}_\alpha$ are the reciprocal lattice vectors and $-N_\alpha/2 < n_\alpha \le N_\alpha/2$, where n_α are integers and N_α are now constant even integers. The wavevectors are taken to be in the first Brillouin zone [38].

For the LJ argon and SW silicon systems studied here, the cubic conventional cells are used with four (argon) and eight (silicon) atoms per unit cell. For the MD simulations of LJ argon and SW silicon, cubic simulation domains are used (i.e., $N_1 = N_2 = N_3 = N_0$) [1, 25, 27]. For the CNT, the Brillouin zone is one-dimensional, so that $N_1 = N_2 = 1$, and we take $N_3 = 50$ [33].

A.3.2   Phonon Lifetimes and Frequencies

Once the allowed wavevectors are specified, the atomic velocities from an MD simulation can be used to calculate Φ' using Equation (A.4). To calculate Φ [Equation (A.18)], (WORK) require the phonon mode eigenvector, which can be obtained using harmonic lattice dynamics calculations and the finite temperature lattice constant (i.e., quasi-harmonic lattice dynamics calculations) [7]. The Φ and Φ' methods can used for any material system where there are available interatomic potentials.

The phonon frequencies and lifetimes are found by fitting the spectral curves Φ and Φ' with Lorentzian functions using a non-linear least squares method. Both of these phonon properties are independent of the Lorentzian peak magnitude. For Φ', the different polarizations at a given wavevector are superimposed by definition of Equation (A.4). The different polarizations can be fit individually using single Lorentzian peaks or as a superposition of peaks. At high temperatures, the broadening of the peaks from different polarizations can make it difficult to uniquely locate the peaks in Φ'. Knowledge of the quasi-harmonic frequencies is necessary to identify the unique peaks in Φ' as well as degeneracies [1, 41].

Φ has the advantage that degenerate and nearly degenerate polarizations can be isolated and fit individually. The uncertainty in the predicted phonon frequencies is on the order of the frequency resolution used to perform the fast Fourier transforms required to evaluate Φ and Φ', which is $10^2 - 10^4$ less than the phonon frequencies studied in this work (see Sections A.4.1, A.4.2, and A.4.3). At the temperatures studied in this work, we find that fitting single or simultaneous peaks in either Φ or Φ' results in less than five percent difference in the predicted lifetimes. The uncertainty from fitting the Lorentzian functions is between five and ten percent of the predicted
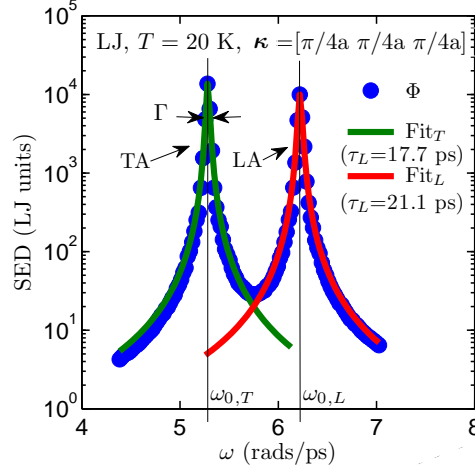
Figure A.1: The SED (using Φ) for the first three polarizations at the wavevector $[\pi/4a, \pi/4a, \pi/4a]$ for LJ argon at a temperature of 20 K. There are two degenerate transverse acoustic (TA) polarizations and one longitudinal acoustic (LA) polarization. When fitting the SED, the different polarizations can be fit individually using single Lorentzian peaks or as a superposition of polarizations. Here the two peaks are fit individually with Φ plotted as a superposition. The predicted lifetimes, which are inversely proportional to Γ are provided in the legend.

lifetimes, with the error increasing with increasing temperature.[1]

To illustrate the procedure, Φ was calculated for LJ argon (Section A.4.1) with $N_0 = 8$ and $T = 20$ K, where T is temperature. Φ for the three modes of lowest frequency and wavevector $[\pi/4a, \pi/4a, \pi/4a]$ is shown in Fig. A.1. The lower-frequency peak corresponds to the two degenerate transverse acoustic modes, while the higher frequency peak corresponds to the longitudinal acoustic mode [7].

A.3.3 Thermal Conductivity

Once the frequencies and lifetimes of all phonon modes in the first Brillouin zone are obtained, the bulk thermal conductivity in direction $\mathbf{n}$, $k_\mathbf{n}$, can be calculated from [42]

$$k_\mathbf{n} = \sum_{\boldsymbol{\kappa}} \sum_{\nu} c_{ph}\binom{\boldsymbol{\kappa}}{\nu} v_{g,\mathbf{n}}^2\binom{\boldsymbol{\kappa}}{\nu} \tau\binom{\boldsymbol{\kappa}}{\nu} . \tag{A.10}$$

Here, c_{ph} is the phonon volumetric specific heat and $v_{g,\mathbf{n}}$ is the component of the group velocity vector in direction $\mathbf{n}$. Since the systems we consider are classical and obey Maxwell-Boltzmann statistics [43], the specific heat is k_B per mode in the harmonic limit, where k_B is the Boltzmann

---

[1]The range of data must be selected when fitting the Lorentzian functions to Φ or Φ'. This range should be large enough for the Lorentzian functions to decrease significantly from their value at half-width at half-maximum, where the linewidth is specified, but not too large as to pick up noise. The error in predicting the lifetime is obtained by varying the range of data used to fit the Lorentzian function.

constant. As temperature increases, anharmonicity causes the mode specific heats to deviate from k_{B} [25]. The effect is small for the systems and temperatures studied here. For LJ argon, the mode-averaged specific heat has been predicted to be $0.95k_{\mathrm{B}}$ per mode at a temperature of 40 K and approaches k_{B} with decreasing temperature [25]. For SW silicon at a temperature of 300 K, the predicted mode-averaged specific heat is $1.01k_{\mathrm{B}}$ per mode [30]. For the CNT at $T = 300$ K, we predict the mode-averaged specific heat to be $1.03k_{\mathrm{B}}$ per mode. Because we do not have mode-dependent specific heats, we take the specific heat to be k_{B} per mode for the three systems studied (argon, silicon, and CNT). The group velocity vector is the gradient of the dispersion curve (i.e., $\partial\omega/\partial\boldsymbol{\kappa}$) and can be calculated from the frequencies and wavevectors using finite differences. In this work, the group velocities are calculated using the frequencies from quasi-harmonic lattice dynamics calculations because a smaller finite difference in wavevector can be used than what is available from the MD simulations (see Section A.3.1). [2]

A.3.4   Computational Cost

The computational cost of evaluating Equation (A.4) is less than that for Equation (A.18) by a factor of $3b$, where b is the number of atoms in the unit cell. For bulk crystals, the number of atoms in the unit cell is typically small ($b < 10$). For the (8,8) CNT system, $b = 32$ and evaluating Φ' is two orders of magnitude less expensive than evaluating Φ.

To calculate the phonon lifetimes, the MD simulation time should be an order of magnitude longer than the longest phonon lifetime [44]. If only the phonon frequencies are required, however, the location of the peaks in Φ and Φ' develop in a time on the order of the inverse of the phonon frequency, $1/\omega_0(^{\boldsymbol{\kappa}}_{\nu})$. For the systems studied here, this time can be two to five orders of magnitude less than the time needed to develop the lifetimes.

Fitting Φ' becomes challenging at higher temperatures, when the phonon linewidths broaden and become comparable to the spacing between mode frequencies. The cost of fitting Φ' can be reduced by fitting the peaks from all allowed wavevectors in the system simultaneously, but the error associated with this procedure is unknown [36]. We find that a semi-automated procedure, whereby the fits are visualized, is necessary to ensure that all peaks are fit correctly. While the computational cost of fitting Φ' is much smaller than the computational cost of calculating Φ', the semi-automated fitting procedure can be of similar time cost to the user. The cost of fitting Φ is much smaller because the different polarization peaks can be isolated and the fitting can be fully automated.

---

[2]The anharmonic frequency shift affects the group velocity. McGaughey and Kaviany find that anharmonic and quasi-harmonic predictions of the group velocity differ for LJ Argon by less than one percent at a temperature of 50 K and that the difference decreases with decreasing temperature [25]. The anharmonic frequency shifts are on average a few percent for LJ argon at a temperature of 40 K and are less for the other temperatures and systems studied here.

A.4   Case Studies

A.4.1   Lennard-Jones Argon

We now use MD simulation to compare the SED, phonon properties, and thermal conductivity calculated for LJ argon using Φ and Φ'. The MD simulations are performed using LAMMPS [**?**]. A truncated and shifted potential cutoff scheme is used with a cutoff radius of 8.5 $\mathring{A}$. The quasi-harmonic phonon frequencies, eigenvectors, and group velocities are generated using GULP [**?**]. We consider temperatures of 5, 20, and 40 K at zero-pressure with lattice constants of 5.278, 5.315, and 5.371 $\mathring{A}$. For LJ argon, Turney et al. found that lattice dynamics-based predictions of thermal conductivity (e.g., by anharmonic lattice dynamics or Φ) start to diverge from MD-based predictions (e.g., from the direct or Green-Kubo methods) above half the melting temperature ($T_{\text{melt}} \approx 80$ K) [1]. Here, we limit the temperature to below half the melting temperature for the three systems studied (argon, silicon, and CNT).

The MD system consists of $N_1 \times N_2 \times N_3 = 8^3 = 512$ conventional cubic unit cells for a total of 2048 atoms ($b = 4$ atoms). Using a 4.285 fs time step, the system is equilibrated for 2^{20} time steps before collecting data every 2^5 time steps for an additional 2^{20} time steps in the NVE ensemble (constant number of atoms, system volume, and total system energy) [43]. The sampling rate must be high enough to capture the highest phonon frequency in the system. The sampling rate and total run time are chosen in powers of two as a convenience in performing the fast Fourier transforms required to efficiently evaluate Φ and Φ'. The same MD simulation data are used to calculate Φ and Φ'. Five simulations with different initial conditions are performed and the Φ and Φ' values are averaged before the peak fitting. Φ and Φ' are further averaged over degenerate wavevectors in the Brillouin zone, reducing the wavevectors to the first octant [45].

The SED (Φ and Φ') for the wavevector [$\pi/2a$,0,0] is presented in Fig. A.2 for all three temperatures (the edge of the Brillouin zone is at [π/a,0,0]). For Φ, the spectral curve is plotted as a superposition over the twelve phonon polarizations, with degeneracy reducing the number of peaks to seven. Overall, Φ' does not equal the total phonon spectral energy density Φ, but the major features are similar. At all temperatures there are linewdith variations between the two spectral curves. The peak magnitudes become comparable for Φ and Φ' as the temperature increases. The phonon frequencies and lifetimes extracted for all allowed wavevectors in the first Brillouin zone using Φ and Φ' at each of the three temperatures are compared on a mode-by-mode basis in Figs. A.3(a), A.3(b), and A.3(c). There, ω_0, ω_0', τ, and τ' refer to the mode properties predicted using Φ and Φ'. The phonon frequencies agree well at all three temperatures, with increasing scatter at high temperatures and high frequencies. This scatter is due to the high-frequency peak broadening seen in Fig. A.2 at $T = 40$ K, which can force peaks close in frequency for Φ' to be fit as a single Lorentzian function. The frequencies predicted by Φ and Φ' include the effects of anharmonicity, which increase the frequencies compared to the quasi-harmonic predictions [1, 41]. The agreement between the frequencies predicted from Φ and Φ' is explained in (REF) (WORK).

The lifetimes show large scatter between Φ and Φ' on a mode-by-mode basis, with increasing scatter at high temperature that shows no systematic difference. The scatter at high frequencies is in part due to the peak broadening seen in Fig. A.2, which can force peaks close in frequency for Φ' to be fit as a single Lorentzian function with a single lifetime. The broadening does not
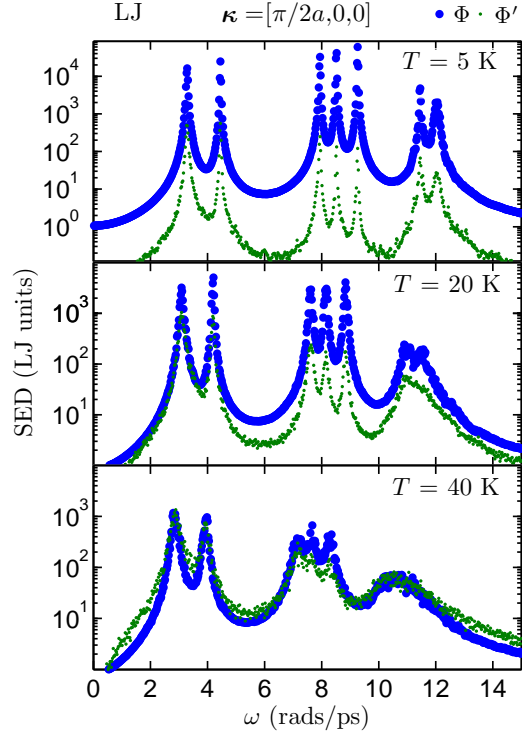
Figure A.2: The phonon spectral energy density (Φ) is plotted as larger blue circles. The proposed alternative expression for the phonon spectral energy density (Φ') is plotted as smaller green points. The wavevector is ($\pi/2a$,0,0). Note that peak broadening at higher temperatures and frequencies above 10 rads/ps can force peaks close in frequency for Φ' to be fit as a single Lorentzian function. Φ does not suffer from this issue since the broadened peaks can be fit individually.

Table A.1: Thermal conductivity values in W/m-K predicted using the Φ, Φ', and Green-Kubo methods. The predictions for Φ and Green-Kubo for the LJ system are in good agreement with those from other atomistic simulation methods [1] while those from Φ' differ and show no consistent behavior. The uncertainties in the predicted thermal conductivities for Φ and Φ' come predominantly from the finite simulation-size scaling procedure (see Ref. [1, 2]), where the phonon properties and thermal conductivity are predicted for increasing system sizes ($N_1 = N_2 = N_3$) to extrapolate a bulk thermal conductivity. For SW silicon and the CNT, the extrapolation procedure is not performed.

T (K)	Green-Kubo	Φ	Φ'
LJ (bulk)			
5	8.0 ± 0.30	7.9 ± 0.42	5.8 ± 0.31
20	1.3 ± 0.15	1.2 ± 0.07	1.0 ± 0.10
40	0.45 ± 0.07	0.47 ± 0.03	0.49 ± 0.05
SW ($N_1 = N_2 = N_3 = 6$)			
300		322 ± 16	396 ± 38
CNT ($N_1 = N_2 = 1, N_3 = 50$)			
300		428 ± 21	398 ± 40

affect fitting at low frequencies, where the linewidths are much smaller than the peak spacings. There, any scatter comes solely from the difference between Φ and Φ'.

The phonon properties are then used to predict thermal conductivity using Equation (A.10). The results are presented in Table A.1. The bulk thermal conductivities provided in Table A.1 are predicted using the finite simulation-size scaling procedure discussed in [1]. The bulk thermal conductivities predicted from Φ' are smaller and outside the uncertainty for those predicted from Φ for temperatures of 5 and 20 K. While the bulk thermal conductivities at a temperature of 40 K agree within their uncertainties, the predicted mode-by-mode lifetimes show large scatter [Fig. A.3(c)] and the agreement should be regarded as coincidental.

The disagreement between Φ and Φ' in thermal conductivity comes directly from the differences in the phonon lifetimes. All other properties (frequencies, group velocities, specific heats) are nearly or exactly the same for the two calculations. The bulk thermal conductivities predicted from Φ and Φ' are also compared to predictions from the Green-Kubo method[43] in Table A.1. For $N_1 = N_2 = N_3 = 8$, the thermal conductivity predicted by the Green-Kubo method is converged with respect to the simulation size [25]. The same MD data used to calculate Φ and Φ' is used for the Green-Kubo predictions. For all three temperatures, there is good agreement between the thermal conductivity predictions using Φ and Green-Kubo. For temperatures of 20 and 40 K, there is good agreement between the predictions from Φ, Green-Kubo, and previous reports using non-equilibrium MD, anharmonic lattice dynamics, and time-domain Φ [1].

Figure A.3: Comparison of the phonon frequencies and lifetimes predicted using Φ (ω and τ) and Φ' (ω' and τ') for LJ argon at temperatures of (a) 5 K, (b) 20 K, and (c) 40 K. The phonon frequencies agree well at all three temperatures, while the phonon lifetimes show large scatter.

Figure A.4: Comparison of the phonon frequencies and lifetimes predicted using Φ (ω and τ) and Φ' (ω' and τ') for SW silicon. The phonon frequencies agree well, while the phonon lifetimes show large scatter.

A.4.2   Stillinger-Weber Silicon

We next compare the phonon properties and thermal conductivity predicted from Φ and Φ' for SW silicon [39] at a temperature of 300 K and zero pressure with a lattice constant of 5.437 Å. The SW system is stiffer (larger phonon group velocities, frequencies, and lifetimes) than LJ argon and is an additional test to determine if there is a systematic error in the predictions from Φ'. The MD simulations are performed using LAMMPS [46]. The MD system consists of $N_1 \times N_2 \times N_3 = 6^3 = 216$ conventional unit cells for a total of 1728 atoms ($b = 8$ atoms). The phonon frequencies, eigenvectors, and group velocities are generated using GULP [47].

Using a 0.5 fs timestep, the system is equilibrated for 2^{20} time steps before collecting data every 2^5 time step for 2^{22} time steps in the NVE ensemble [43]. As with the LJ system, the sampling rate is determined by the highest phonon frequency in the system. Five simulations with different initial conditions are performed and the Φ and Φ' values are averaged before the peak fitting. Φ and Φ' are further averaged over degenerate wavevectors in the Brillouin zone, reducing the wavevectors to the first octant [45].

The extracted phonon frequencies and lifetimes are plotted in Fig. A.4. As with the LJ system, the phonon frequencies are predicted accurately by Φ' but the lifetimes show large scatter on a mode-by-mode basis. For the system size studied, Φ' predicts a larger thermal conductivity than Φ outside the prediction uncertainties, in contrast to the LJ system (see Table A.1). The disagreement in thermal conductivity comes directly from the phonon lifetimes.
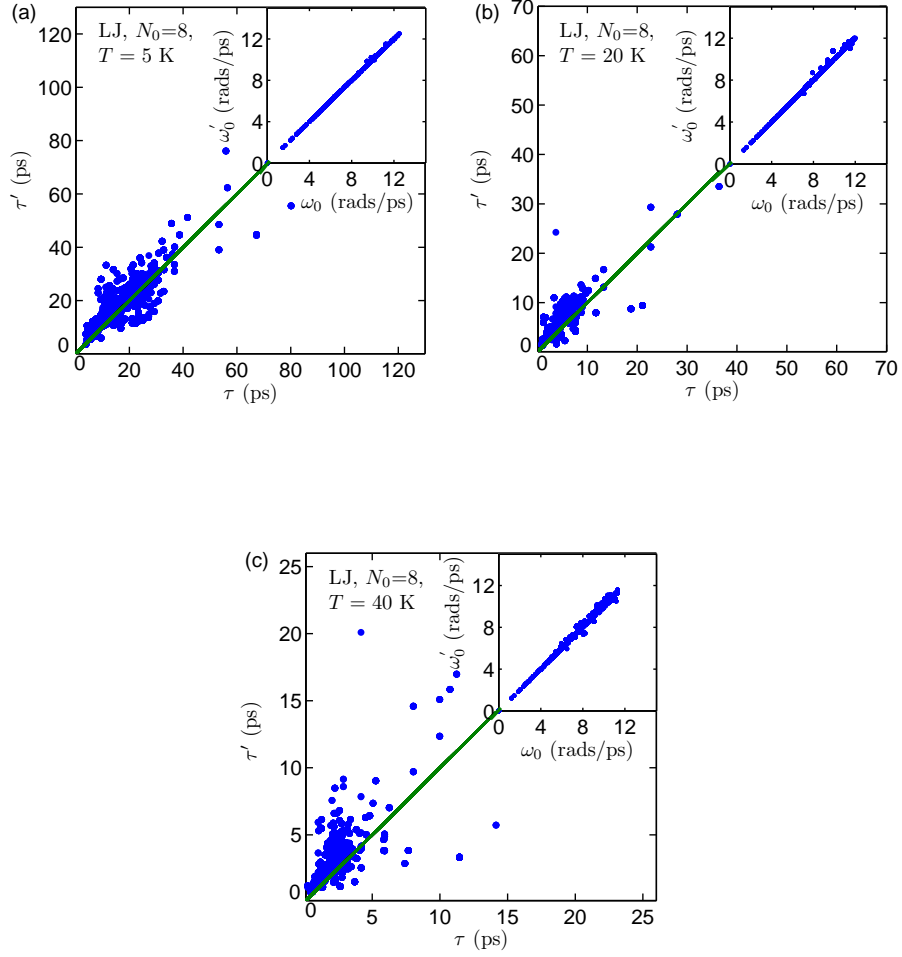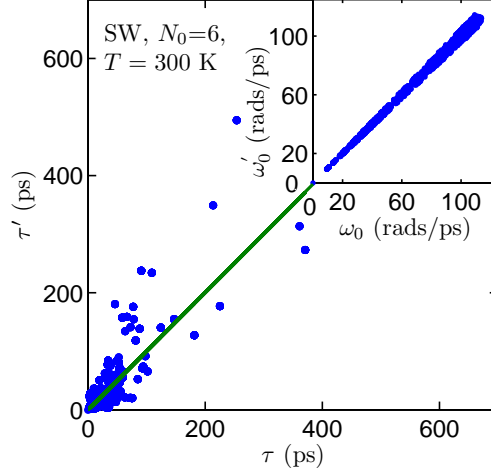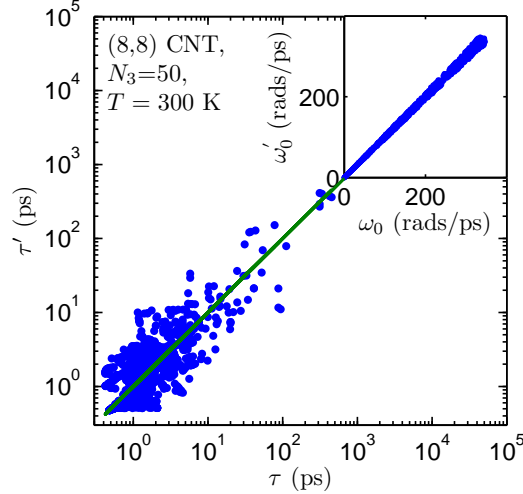
Figure A.5: Comparison of the phonon frequencies and lifetimes predicted using Φ (ω, τ) and Φ' (ω', τ') for a (8,8) CNT modeled using the REBO potential. The phonon frequencies agree well, while the phonon lifetimes show large scatter.

A.4.3 Carbon Nanotube

Finally, we compare the phonon properties and thermal conductivities predicted by Φ and Φ' for an (8,8) CNT (diameter of 1.10-nm and length of 12.3 nm) at a temperature of 300 K and zero pressure [33]. The interactions in the CNT system are modeled using the REBO potential without the four-body interaction term [?]. The MD simulations are performed using an in-house code. The MD system consists of 1600 atoms (32 atoms/unit cell). The phonon frequencies, eigenvectors, and group velocities are generated using an in-house code. The purpose of simulating this system is to check the results of Thomas et al. [33] (who used Φ' and non-equilibrium MD), and to compare the predictions of Φ' and Φ.

Using a 1.0 fs timestep, the system is equilibrated for 2^{20} time steps before collecting data every 2^3 time step for 2^{22} time steps in the NVE ensemble [43]. As with the LJ and SW systems, the sampling rate is determined by the highest phonon frequency in the system. Five simulations with different initial conditions are performed and the Φ and Φ' values are averaged before the peak fitting. Since the Brillouin zone of the CNT is one-dimensional, Φ and Φ' are further averaged over directionally-degenerate wavevectors.

The phonon frequencies and lifetimes for the allowed wavevectors in the one-dimensional Brillouin zone are shown in Fig. A.5. Like the LJ and SW silicon systems, the phonon frequencies can be predicted accurately by Φ', but the lifetimes show large scatter. The estimated thermal conductivity of the CNT predicted using Φ' is in agreement with the results of Thomas et al. [33]. The thermal conductivity predicted by Φ' is less than that predicted by Φ, but not outside their uncertainties.

A.5   Summary

We presented the correct phonon SED, Φ, and its relation to the phonon frequencies and lifetimes. We then presented an alternative formulation to the phonon spectral energy density, Φ', which does not require the phonon mode eigenvectors. Because Φ' does not contain the eigenvectors, this alternative formulation does not represent the phonon spectral energy density, but does contain information about the phonon dispersion as the temperature approaches 0 K (see (REF) (WORK)).

We then calculated the phonon SED for LJ argon, SW silicon, and a CNT modeled with the REBO potential using Φ and Φ'. The phonon frequencies and lifetimes predicted from Φ and Φ' are shown in Figs. A.3, A.4 and A.5. The frequencies are in good agreement between the two SED methods, while the lifetimes show large scatter.

The phonon SED Φ is well-defined theoretically, while Φ' does not properly map to the phonon energies since it is missing the phonon mode eigenvector. We deduce that this is the reason Φ' does not accurately predict the phonon lifetimes. It is surprising how close the predicted thermal conductivities can be using Φ and Φ' (LJ at $T = 40$ K and the CNT results). The thermal conductivities predicted by Φ and Φ', however, show no consistency for the three systems studied.

The most important predictions are the mode-by-mode phonon properties. Of particular importance are the lifetimes, which are the key input for Boltzmann transport equation-based models [23]. Thus, we do not recommend Φ' for predicting phonon lifetimes or thermal conductivity. Any agreement in thermal conductivity predictions between atomistic studies[33] and experiment [35**?**] should be regarded as coincidental, and the phonon lifetime reductions predicted for systems with additional scattering methods [33, 36] should only be interpreted qualitatively. The use of Φ' in future work is discouraged and we reccomend the use of Φ.

A.6   Derivation of Phonon Spectral Energy Density, Φ

(WORK)

To derive the correct expression for the phonon SED, Φ, we begin with harmonic lattice dynamics theory.[6, 7] The derivation outlined here is presented in detail in Appendix A.6.

In reciprocal space, the system Hamiltonian, H, is

$$
\begin{aligned}
H &= \frac{1}{2}0 \sum_{\alpha,b,l}^{3,n,N} 1 \sum_{\alpha,b}^{3,n} \sum_{\boldsymbol{\kappa},\nu}^{N,3n} \left[\dot{q}^*(^{\boldsymbol{\kappa}}_{\nu};t)\, \dot{q}(^{\boldsymbol{\kappa}}_{\nu};t) + \omega_0^2(^{\boldsymbol{\kappa}}_{\nu})\, q^*(^{\boldsymbol{\kappa}}_{\nu};t)\, q(^{\boldsymbol{\kappa}}_{\nu};t) \right] \\
&= 0 \sum_{\alpha,b,l}^{3,n,N} 1 \sum_{\alpha,b}^{3,n} \sum_{\boldsymbol{\kappa},\nu}^{N,3n} \left[T(^{\boldsymbol{\kappa}}_{\nu};t) + V(^{\boldsymbol{\kappa}}_{\nu};t) \right],
\end{aligned}
\tag{A.11}
$$

where t is time, $\omega_0(^{\boldsymbol{\kappa}}_{\nu})$ is the frequency of the phonon mode denoted by wave vector $\boldsymbol{\kappa}$ and dispersion branch ν, and N and n are the total number of unit cells and the number of atoms in the unit cell. The Hamiltonian is the total system energy and is the sum of the mode- and time-dependent kinetic and potential energies, $T(^{\boldsymbol{\kappa}}_{\nu};t)$ and $V(^{\boldsymbol{\kappa}}_{\nu};t)$. The phonon normal mode coordinate, $q(^{\boldsymbol{\kappa}}_{\nu};t)$

and its time derivative, $q(^{\boldsymbol{\kappa}}_{\nu}; t)$, are given by

$$q(^{\boldsymbol{\kappa}}_{\nu}; t) = 00 \sum_{\alpha,b,l}^{3,n,N} 01 \sum_{\alpha,b}^{3,n} \sum_{\boldsymbol{\kappa},\nu}^{N,3n} \sqrt{\frac{m_b}{N}} u_\alpha(^l_b; t) \, e^*(^{\boldsymbol{\kappa}\ b}_{\nu\ \alpha}) \exp[i\boldsymbol{\kappa} \cdot \mathbf{r}_0(^{lal}_{0b0})] \tag{A.12}$$

and

$$\dot{q}(^{\boldsymbol{\kappa}}_{\nu}; t) = 00 \sum_{\alpha,b,l}^{3,n,N} 01 \sum_{\alpha,b}^{3,n} \sum_{\boldsymbol{\kappa},\nu}^{N,3n} \sqrt{\frac{m_b}{N}} \dot{u}_\alpha(^l_b; t) \, e^*(^{\boldsymbol{\kappa}\ b}_{\nu\ \alpha}) \exp[i\boldsymbol{\kappa} \cdot \mathbf{r}_0(^{lal}_{0b0})], \tag{A.13}$$

where m_b is the mass of the bth atom in the unit cell and $\mathbf{r}_0(^{lal}_{0b0})$ is the equilibrium position vector of the lth unit cell. The α-component of the displacement from equilibrium, $u_\alpha(^l_b; t)$, and velocity, $\dot{u}_\alpha(^l_b; t)$, of the bth atom in the lth unit cell are time-dependent and are related to the phonon mode coordinates through the time-independent eigenvector that has components $e(^{\boldsymbol{\kappa}\ b}_{\nu\ \alpha})$.

The expectation value of the kinetic energy of each normal mode in the time domain is

$$\langle T(^{\boldsymbol{\kappa}}_{\nu}) \rangle = \lim_{\tau_0 \to \infty} \frac{1}{2\tau_0} \int_0^{\tau_0} \dot{q}^*(^{\boldsymbol{\kappa}}_{\nu}; t) \, \dot{q}(^{\boldsymbol{\kappa}}_{\nu}; t) \, dt. \tag{A.14}$$

The expectation value of the kinetic energy of the normal mode can be transformed from the time domain to the frequency domain by Parseval's theorem,[40]

$$T(^{\boldsymbol{\kappa}}_{\nu}; \omega) = \lim_{\tau_0 \to \infty} \frac{1}{2\tau_0} \left| \frac{1}{\sqrt{2\pi}} \int_0^{\tau_0} \dot{q}(^{\boldsymbol{\kappa}}_{\nu}; t) \exp(-i\omega t) dt \right|^2. \tag{A.15}$$

Starting from Eq. (A.15) and following the derivation in Appendix A.6, one arrives at the expression for the SED of a single phonon mode,

$$T(^{\boldsymbol{\kappa}}_{\nu}; \omega) = \frac{C_0(^{\boldsymbol{\kappa}}_{\nu})}{2} \frac{\Gamma(^{\boldsymbol{\kappa}}_{\nu})/\pi}{[\omega_0(^{\boldsymbol{\kappa}}_{\nu}) - \omega]^2 + \Gamma^2(^{\boldsymbol{\kappa}}_{\nu})}, \tag{A.16}$$

which is a Lorentzian function with center at $\omega_0(^{\boldsymbol{\kappa}}_{\nu})$ and a half-width at half-maximum (linewidth) of $\Gamma(^{\boldsymbol{\kappa}}_{\nu})$. The constant $C_0(^{\boldsymbol{\kappa}}_{\nu})$ is defined in Eq. (A.31) in Appendix A.6. We know from anharmonic lattice dynamics theory that the phonon linewidth is related to the phonon lifetime, $\tau(^{\boldsymbol{\kappa}}_{\nu})$, by[24, 28]

$$\tau(^{\boldsymbol{\kappa}}_{\nu}) = \frac{1}{2\Gamma(^{\boldsymbol{\kappa}}_{\nu})}. \tag{A.17}$$

The MD simulations we perform here are classical. For a classical system in the harmonic limit (i.e., temperature approaching zero) there is an equipartition of energy and $\sum_\nu^{3n} T(^{\boldsymbol{\kappa}}_{\nu}; \omega) = \sum_\nu^{3n} V(^{\boldsymbol{\kappa}}_{\nu}; \omega)$.[43] In an anharmonic system (i.e., a MD simulation), the assumption of equipartition of energy can be tested by predicting the system-level specific heat (see Section A.3.3). By assuming equipartition of energy, the phonon SED at a particular wavevector is

$$\Phi(\boldsymbol{\kappa}, \omega) = 2 \sum_\nu^{3n} T(^{\boldsymbol{\kappa}}_{\nu}; \omega) = \sum_\nu^{3n} C_0(^{\boldsymbol{\kappa}}_{\nu}) \frac{\Gamma(^{\boldsymbol{\kappa}}_{\nu})/\pi}{[\omega_0(^{\boldsymbol{\kappa}}_{\nu}) - \omega]^2 + \Gamma^2(^{\boldsymbol{\kappa}}_{\nu})}, \tag{A.18}$$

which is a superposition of $3n$ Lorentzian functions with centers at $\omega_0(^{\boldsymbol{\kappa}}_{\nu})$ (one for each polarization). For simplicity, we refer to $\Phi(\boldsymbol{\kappa}, \omega)$ as Φ. Given a set of atomic velocities, Φ can be calculated using Eq. (A.13) and (A.15), and then fit using Eq. (A.18) to extract the phonon properties $\omega_0(^{\boldsymbol{\kappa}}_{\nu})$ and $\tau(^{\boldsymbol{\kappa}}_{\nu})$.

Previous work using normal mode analysis has represented the phonon energy in the time domain, [1, 2, 24, 25, 29, 30] while Φ is a representation of the phonon energy in the frequency domain. The time- and frequency-domain approaches are mathematically equivalent by use of the Wiener-Khinchin theorem. [36, 40] The frequency-domain approach has the advantage of predicting both the phonon lifetime and frequency by fitting a simpler function than required in the time-domain approach.

(WORK)

We start from Eq. (A.13) and follow the formulation of anharmonic lattice dynamics theory. [5, 6, 7?] In an anharmonic system, the phonon populations fluctuate about the equilibrium distribution function.[6] The phonon mode coordinate for the mode described by $(\boldsymbol{\kappa}, \nu)$ and its time derivative can be written as

$$q(^{\boldsymbol{\kappa}}_{\nu}; t) = q_{SS}(^{\boldsymbol{\kappa}}_{\nu}; t) + q_T(^{\boldsymbol{\kappa}}_{\nu}; t) \tag{A.19}$$

and

$$\dot{q}(^{\boldsymbol{\kappa}}_{\nu}; t) = \dot{q}_{SS}(^{\boldsymbol{\kappa}}_{\nu}; t) + \dot{q}_T(^{\boldsymbol{\kappa}}_{\nu}; t). \tag{A.20}$$

The steady-state (SS) and transient (T) parts and their time derivatives are given by

$$\begin{aligned} q_{SS}(^{\boldsymbol{\kappa}}_{\nu}; t) = &C_1(^{\boldsymbol{\kappa}}_{\nu}) \exp[i\omega_0(^{\boldsymbol{\kappa}}_{\nu})\, t] \\ &+ C_2(^{\boldsymbol{\kappa}}_{\nu}) \exp[-i\omega_0(^{\boldsymbol{\kappa}}_{\nu})\, t], \end{aligned} \tag{A.21}$$

$$\begin{aligned} q_T(^{\boldsymbol{\kappa}}_{\nu}; t) = &\exp[-\Gamma(^{\boldsymbol{\kappa}}_{\nu})\, |t|]\{C_3(^{\boldsymbol{\kappa}}_{\nu}) \exp[i\omega_0(^{\boldsymbol{\kappa}}_{\nu})\, t] \\ &- C_4(^{\boldsymbol{\kappa}}_{\nu}) \exp[-i\omega_0(^{\boldsymbol{\kappa}}_{\nu})\, t]\}, \end{aligned} \tag{A.22}$$

$$\dot{q}_{SS}(^{\boldsymbol{\kappa}}_{\nu}; t) = i\omega_0 \left\{ C_1(^{\boldsymbol{\kappa}}_{\nu}) \exp[i\omega_0(^{\boldsymbol{\kappa}}_{\nu})\, t] - C_2(^{\boldsymbol{\kappa}}_{\nu}) \exp[-i\omega_0(^{\boldsymbol{\kappa}}_{\nu})\, t] \right\}, \tag{A.23}$$

and

$$\begin{aligned} \dot{q}_T(^{\boldsymbol{\kappa}}_{\nu}; t) = &\exp[-\Gamma(^{\boldsymbol{\kappa}}_{\nu})\, |t|]\{C_3(^{\boldsymbol{\kappa}}_{\nu}) [i\omega_0(^{\boldsymbol{\kappa}}_{\nu}) - \Gamma(^{\boldsymbol{\kappa}}_{\nu})] \exp[i\omega_0(^{\boldsymbol{\kappa}}_{\nu})\, t] \\ &- C_4(^{\boldsymbol{\kappa}}_{\nu}) [i\omega_0(^{\boldsymbol{\kappa}}_{\nu}) + \Gamma(^{\boldsymbol{\kappa}}_{\nu})] \exp[-i\omega_0(^{\boldsymbol{\kappa}}_{\nu})\, t] \right\}, \end{aligned} \tag{A.24}$$

where the Cs are constants and $\omega_0(^{\boldsymbol{\kappa}}_{\nu})$ and $\Gamma(^{\boldsymbol{\kappa}}_{\nu})$ are the phonon mode frequency and linewidth. The transient part describes the creation of an excess in the population of a phonon mode for $t < 0$ and its decay back to equilibrium for $t > 0$.

Phonon population fluctuations are commonly modeled using the excitation and decay of a single phonon mode (i.e., the single mode relaxation time approximation). In a real system, there will be multiple phonons in each mode that simultaneously grow or decay with time. Thus, dealing only with $\dot{q}$, we let

$$\begin{aligned} \dot{q}(^{\boldsymbol{\kappa}}_{\nu}; t) = &\sum_j i \exp[-\Gamma(^{\boldsymbol{\kappa}}_{\nu})\, |t - t_j|] \times \\ &\{A_j(^{\boldsymbol{\kappa}}_{\nu}) [\omega_0(^{\boldsymbol{\kappa}}_{\nu}) + i\Gamma(^{\boldsymbol{\kappa}}_{\nu})] \exp[i\omega_0(^{\boldsymbol{\kappa}}_{\nu}) (t - t_j)] \\ &- B_j(^{\boldsymbol{\kappa}}_{\nu}) [\omega_0(^{\boldsymbol{\kappa}}_{\nu}) - i\Gamma(^{\boldsymbol{\kappa}}_{\nu})] \exp[-i\omega_0(^{\boldsymbol{\kappa}}_{\nu}) (t - t_j)] \}, \end{aligned} \tag{A.25}$$

where many phonons in each mode, indexed by j, are simultaneously being created and destroyed. The phonons grow for $t < t_j$, decay for $t > t_j$, and A_j and B_j are constants. We are not concerned with the values of t_j, A_j, and B_j, though they should satisfy the long-time average $\langle \dot{q}^*(^{\boldsymbol{\kappa}}_{\nu}; t)\, \dot{q}(^{\boldsymbol{\kappa}}_{\nu}; t) \rangle = \langle \dot{q}^*_{SS}(^{\boldsymbol{\kappa}}_{\nu}; t)\, \dot{q}_{SS}(^{\boldsymbol{\kappa}}_{\nu}; t) \rangle$.

The expectation value of the kinetic energy of the normal mode in the time domain is

$$\langle T(^{\boldsymbol{\kappa}}_{\nu}) \rangle = \frac{1}{2} \lim_{\tau_0 \to \infty} \frac{1}{\tau_0} \int_0^{\tau_0} \dot{q}^*(^{\boldsymbol{\kappa}}_{\nu}; t)\, \dot{q}(^{\boldsymbol{\kappa}}_{\nu}; t)\, dt. \tag{A.26}$$

The expectation value of the kinetic energy of the normal mode can be transformed from the time domain to the frequency domain by Parseval's theorem,[40] giving

$$T(^{\boldsymbol{\kappa}}_{\nu}; \omega) = \lim_{\tau_0 \to \infty} \frac{1}{2\tau_0} \left| \frac{1}{\sqrt{2\pi}} \int_0^{\tau_0} \dot{q}(^{\boldsymbol{\kappa}}_{\nu}; t) \exp(-i\omega t) dt \right|^2. \tag{A.27}$$

By substituting Eq. (A.25) into Eq. (A.27) and performing the time integration we find

$$T(^{\boldsymbol{\kappa}}_{\nu}; \omega) = \frac{1}{16\pi\tau_0} \left| \sum_j \exp[-i\omega t_j] \left\{ A_j(^{\boldsymbol{\kappa}}_{\nu}) \frac{\omega_0(^{\boldsymbol{\kappa}}_{\nu}) + i\Gamma(^{\boldsymbol{\kappa}}_{\nu})}{\omega_0(^{\boldsymbol{\kappa}}_{\nu}) - \omega + i\Gamma(^{\boldsymbol{\kappa}}_{\nu})} \right. \right.$$
$$\left. \left. + B_j(^{\boldsymbol{\kappa}}_{\nu}) \frac{\omega_0(^{\boldsymbol{\kappa}}_{\nu}) - i\Gamma(^{\boldsymbol{\kappa}}_{\nu})}{\omega_0(^{\boldsymbol{\kappa}}_{\nu}) + \omega - i\Gamma(^{\boldsymbol{\kappa}}_{\nu})} \right\} \right|^2. \tag{A.28}$$

We are primarily interested in values of ω where $\omega \approx \omega_0$ when $\Gamma << \omega_0$ (this condition is met for the three systems studied here). When $\omega \approx \omega_0$, the term involving A_j becomes large and the term involving B_j can be neglected (alternatively, we could ignore the term involving A_j when $\omega \approx -\omega_0$). Hence, we find

$$T(^{\boldsymbol{\kappa}}_{\nu}; \omega) = \frac{1}{16\pi\tau_0} \sum_j \sum_{j'} \cos\left[\omega(t_{j'} - t_j)\right] A_j(^{\boldsymbol{\kappa}}_{\nu})\, A_{j'}(^{\boldsymbol{\kappa}}_{\nu})$$
$$\times \frac{\omega_0^2(^{\boldsymbol{\kappa}}_{\nu}) + \Gamma^2(^{\boldsymbol{\kappa}}_{\nu})}{\Gamma(^{\boldsymbol{\kappa}}_{\nu})} \frac{\Gamma(^{\boldsymbol{\kappa}}_{\nu})}{[\omega_0(^{\boldsymbol{\kappa}}_{\nu}) - \omega]^2 + \Gamma^2(^{\boldsymbol{\kappa}}_{\nu})}. \tag{A.29}$$

We arrive at the expression for the phonon spectral energy density for the wavevector $\boldsymbol{\kappa}$ by summing Eq. (A.29) over the different polarizations ν,

$$\Phi(\boldsymbol{\kappa}, \omega) = 2 \sum_{\nu}^{3n} T(^{\boldsymbol{\kappa}}_{\nu}; \omega) = \sum_{\nu}^{3n} C_0(^{\boldsymbol{\kappa}}_{\nu}) \frac{\Gamma(^{\boldsymbol{\kappa}}_{\nu})/\pi}{[\omega_0(^{\boldsymbol{\kappa}}_{\nu}) - \omega]^2 + \Gamma^2(^{\boldsymbol{\kappa}}_{\nu})}, \tag{A.30}$$

where the factor of two comes from equipartition of kinetic and potential energy (valid for a harmonic classical system, see Section A.3.3), and

$$C_0(^{\boldsymbol{\kappa}}_{\nu}) = \sum_j \sum_{j'} \cos\left[\omega(t_{j'} - t_j)\right] A_j(^{\boldsymbol{\kappa}}_{\nu})\, A_{j'}(^{\boldsymbol{\kappa}}_{\nu}) \frac{\omega_0^2(^{\boldsymbol{\kappa}}_{\nu}) + \Gamma^2(^{\boldsymbol{\kappa}}_{\nu})}{8\tau_0\Gamma(^{\boldsymbol{\kappa}}_{\nu})}. \tag{A.31}$$

Thus, the phonon spectral energy density $\Phi(\boldsymbol{\kappa}, \omega)$ is a superposition of $3n$ Lorentzian functions with centers at $\omega_0(^{\boldsymbol{\kappa}}_{\nu})$ (one for each polarization) with a linewidth (half-width at half-maximum)

of $\Gamma(^{\boldsymbol{\kappa}}_{\nu})$. Φ is a spectral energy density since its integral over all wavevectors and frequencies is the total crystal energy, i.e., the Hamiltonian is

$$H = \int\limits_{V_{BZ}} \int_0^\infty \Phi(\boldsymbol{\kappa}, \omega) d\omega d\boldsymbol{\kappa}, \tag{A.32}$$

where V_{BZ} is the volume of the first Brillouin zone. Like the frequency broadening, there is also a broadening of the SED in wavevector. [**?**] For a finite sampling of the first Brillouin zone, the Hamiltonian can be approximated by

$$H \approx 2 \sum_{\boldsymbol{\kappa},\nu}^{N,3n} \langle T(^{\boldsymbol{\kappa}}_{\nu}; t) \rangle = \sum_{\boldsymbol{\kappa}}^{N} \int_0^\infty \Phi(\omega, \boldsymbol{\kappa}) d\omega. \tag{A.33}$$

A.7 Interpretation of Φ'

(WORK): combine disucssion is book and also on static and dynamic-structure factor. SF can be related to the DOS(cite).

As demonstrated in Section A.4.1, Φ' is not the phonon spectral energy density, Φ, defined by Eq. (A.15). Our findings and those of others, [31, 33, 35, 36**?**] however, suggest that Φ' does contain accurate information about the phonon frequencies. Under the harmonic approximation, the phonons are non-interacting and have no transient response beyond a harmonic oscillation (see Appendix A.6 Eq. (A.20) and (A.24)),

$$\begin{aligned}
\dot{q}(^{\boldsymbol{\kappa}}_{\nu}; t) &= \dot{q}_{SS}(^{\boldsymbol{\kappa}}_{\nu}; t) \\
&= i\omega_0(^{\boldsymbol{\kappa}}_{\nu}) \left\{ C_1(^{\boldsymbol{\kappa}}_{\nu}) \exp[i\omega_0(^{\boldsymbol{\kappa}}_{\nu}) t] - C_2(^{\boldsymbol{\kappa}}_{\nu}) \exp[-i\omega_0(^{\boldsymbol{\kappa}}_{\nu}) t] \right\}.
\end{aligned} \tag{A.34}$$

Inserting Eq. (A.34) into the right hand side of Eq. (A.6) gives

$$\begin{aligned}
&\sum_\alpha^3 \sum_b^n m_b \left| \sum_l^N \int_{-\infty}^\infty \dot{u}_\alpha(^l_b; t) \exp[i\boldsymbol{\kappa} \cdot \mathbf{r}_0(^{lal}_{0b0}) - i\omega t] dt \right|^2 = \\
&\sum_\alpha^3 \sum_b^n \left| \frac{m_b^{3/2}}{\sqrt{N}} \sum_l^N \sum_\nu^{3n} D(^{\boldsymbol{\kappa}\ b}_{\nu\ \alpha}) \exp[i\boldsymbol{\kappa} \cdot \mathbf{r}_0(^{lal}_{0b0})] \delta[\omega_0(^{\boldsymbol{\kappa}}_{\nu}) - \omega] \right|^2,
\end{aligned} \tag{A.35}$$

where $D(^{\boldsymbol{\kappa}\ b}_{\nu\ \alpha}) = i\sqrt{2\pi}\omega_0(^{\boldsymbol{\kappa}}_{\nu}) C_1(^{\boldsymbol{\kappa}}_{\nu}) e^*(^{\boldsymbol{\kappa}\ b}_{\nu\ \alpha})$, δ is the Dirac function, and values of $\omega \leq 0$ are ignored. Thus, at zero temperature Eq. (A.4) is a superposition of Dirac functions at the phonon frequencies $\omega_0(^{\boldsymbol{\kappa}}_{\nu})$.

A.8 Finite Simulation-Size Scaling for Thermal Conductivity

(WORK): add discussion from vc and mfp papers.

For the LJ argon system studied in Section A.4.1, a finite simulation-size scaling procedure [1, 2] is used to compare the thermal conductivity predictions from Φ and Φ' to those from the

Figure A.6: Thermal conductivity predictions for LJ argon calculated using phonon lifetimes predicted by Φ and Φ'. (a) The finite simulation-size scaling extrapolation [1, 2] is used to compare the results to bulk predictions made using the Green-Kubo method. (b) The bulk results for Φ and Green-Kubo are in good agreement temperatures of 20 and 40 K with those of other atomistic simulation methods,[1] while those from Φ' differ (see Table A.1).

Green-Kubo method. The scaling procedure is demonstrated in Fig. A.6. The thermal conductivity is predicted from Φ or Φ' and MD simulations with $N_0 = 4, 6, 8,$ and 10. The bulk conductivity, k_∞, is then estimated by fitting the data to

$$1/k = 1/k_\infty + A/N_0, \tag{A.36}$$

where A is a constant. This procedure is necessary because the first Brillouin zone is only sampled at a finite number of points for a finite simulation size, with no contribution from the volume at its center. To predict a bulk thermal conductivity, it is important to sample points near the Brillouin zone center, where the modes can have large lifetimes and group velocities.[1, 27] As with the extrapolated bulk thermal conductivities at temperatures of 5 and 20 K (see Table A.1), the predicted thermal conductivities at each system size ($N_0 = 4, 6, 8,$ and 10) are systematically smaller and outside the prediction uncertainties for Φ' compared to Φ.

Appendix B

Setting Up Computing Environment

B.1 Setting Up Computing Environment

B.1.1 Setting Up Computing Environment

B.1.2 Setting Up Computing Environment

Linux: world's most widely used software

Linux runs on cell phones to the world's largest supercomputers.

Reccomend the most widely used linux version ubuntu.

Ubuntu is certified on many top PC's from many computer companies There is even a company, system 76, who builds ubuntu-based computers solely.

well-documented, large-community discussion

apple mac OS as it is unix-like.

Wikibooks home

<div align="center">Listing B.1: Some Code</div>

```
public void here() {
        goes().the().code()
}
```

setting up environment: $PATH,

http://en.wikipedia.org/wiki/Environment$_{variable}$

sudo apt-get install gfortran, which gfortran gnu compilers vs intel: gnu freely available tar -zxvf lammps.tar, make serial, sudo apt-get install openmpi, make openmpi

suggested reading:

Statistical Mechanics/Condensed Matter MacQuarrie Ashcroft Wikipedia

Lattice Dynamics Dove: harmonic autocorrelation (DOS), harmonic (dispersion), thermodynamics, structural phase transition, Srivistava: quantum formalism, perturbation theory peierls: ziman: BTE, RTA Wikipedia

Quantum Chemistry Griffiths Quantum Mechanics: Pauli-Exclusion -¿ Exp repulsion Martin Electron Strucutre: DFT Wikipedia

Math Theory/Numerical Methods MacQuarrie Moin Wikipedia

Wikipedia == open source

list of useful packages: pacakges used during this thesis: open-source: lammps, gulp, abinit, qe, vesta, phonopy, ntpy other: vasp

http://www.ks.uiuc.edu/Research/vmd/

other packages: dlpoly, siesta, GAMES, cp2k, boltztrap, PHON,

Useful Linux Commands

google: linux sed

sed, grep, ls, cd, pwd, export/setenv, scp -r, ssh, sudo, nohup, vi, cat, which (program), echo, qstat -u -n, qdel,

Running Linux System Commands in Python

python vs other languages: combines strengths of the 3 important: PERL+java+matlab 1) shell-scripting: controlling the OS, system(cmd), (PERL)

lmp.in.iseed

2) hi-level organization: object-oriented (module.method(input)) (Java) 3) lin alg + numerical methods: numpy.method, scipy.method (fortran, matlab) python deficiencies more about this in the appendix

B.1.3   Preparing Journal Articles and Thesis

Here is a list of experts I used as resources for this work. They will typically answer emails within 24-48 hours:

Alan McGaughey

Jon Malen

Julian Gale, GULP author

Keivan Esfarjani

Joseph Feldman

Junchiro Shiomi

Davide Donadio

Craig Maloney

Jivtesh Garg

me, haha

B.1.4   Coding Languages

As we will see in the dicussion following, there are many languages used for the open-source and lisenced packages(REF) that can be used to study nanoscale transport.

B.1.5   Compiled versus Interpreted

http://en.wikipedia.org/wiki/Compiled$_l anguage$

http://en.wikipedia.org/wiki/Interpreted$_l anguage$

The most commonly used compiled languages are C++ (linux, LAMMPS, spglib) and Fortran: (GULP, quantum espresso, VASP)

A good discussion on the strengths of C++ versus Fortran.

The two most likely interpreted languages you are likely to use are matlab (licesensed)
http://en.wikipedia.org/wiki/MATLAB and python (open-source) http://en.wikipedia.org/wiki/Python$_{(programm}$

The key to maximizing the potential of these languages is by vectorization: using the built-in
"vector" functions and operations provided by the matlab http://www.mathworks.com/help/matlab/matlab$_p$rog/ve
$//faculty.washington.edu/rjl/uwamath583s11/sphinx/notes/html/python_vect.htmlprogramminglibra$

linux/unix shell
excellent c++ tutorial
excellent fortran tutorial
matlab has an excellent built-in guide, google search will typically yield useful results.
matlab
octave

B.1.6   Case-study 1: LJ Argon Molecular Dynamics

The first case study is a single C code to perform Molecular Dynamics on LJ argon. The code is
a serial code with

<div align="center">Listing B.2: Some Code</div>

```
jason@jason−900X3C ˜/ classes /cmu/ molecular_simulation /HW5 ( master )  c++ Argo
```

<div align="center">Listing B.3: Some Code</div>

```
jason@jason−900X3C ˜/ classes /cmu/ molecular_simulation /HW5 ( master )  ./ ArgonM
```

The output is

B.1.7   Case-study 1: LJ Dispersion

B.1.8   Case-study 1: Allen-Feldman Diffusivity Calculation

Two systems, my local laptop:
   http://www.samsung.com/us/computer/series-9-notebooks

<div align="center">Listing B.4: Some Code</div>

```
jason@jason−900X3C ˜/ disorder ( master ) $\$$ cat / proc / cpuinfo
processor        : 0
vendor_id        : GenuineIntel
cpu family       : 6
model            : 58
model name       : Intel (R)  Core (TM)  i5 −3317U CPU @  1.70GHz
stepping         : 9
microcode        : 0x17
cpu MHz          : 782.000
cache size       : 3072 KB
physical id      : 0
siblings         : 4
```

```
core  id          :  0
cpu  cores        :  2
apicid            :  0
initial  apicid   :  0
```

and gilgamesh

http://gilgamesh.cheme.cmu.edu/doc/gilgamesh.html

Listing B.5: Some Code

```
jason@gilgamesh > cat /proc/cpuinfo
processor         :  0
vendor_id         :  AuthenticAMD
cpu  family       :  16
model             :  9
model  name       :  AMD Opteron(tm) Processor 6128 HE
stepping          :  1
cpu  MHz          :  2000.003
cache  size       :  512 KB
physical  id      :  1
siblings          :  8
core  id          :  0
cpu  cores        :  8
apicid            :  16
```

B.1.9   Online Resources

wikipedia

octave

https://en.wikipedia.org/wiki/Lennard-Jones$_{p}otential$

http://www.sklogwiki.org/SklogWiki/index.php/Lennard-Jones$_{m}odel$

we can do better, needs to be organization.

http://nanohub.org/

does not provide good HPC resources.

B.1.10   Latex Resources

http://tex.stackexchange.com/questions/1596/how-to-compile-a-latex-document

http://stackoverflow.com/questions/2461905/compiling-latex-bib-source

http://publish.aps.org/revtex

used

http://kile.sourceforge.net/

http://www.zotero.org/

34

B.1.11 Google Searching

Web-searching.

keywords: integrated development environment (IDE),

B.1.12 Symmetry Discussion

https://github.com/ankitjainmeiitk

http://spglib.sourceforge.net/

Ab initio codes such as abinit and quantum espresso also print the symmetry operations information.

$k_{ij} = k_{ji}$ and $k_{ii} = kjj$ show using symmetry operations

$S = [-100; 010; 001]$

This applies to any vector or tensor property of the crystal.

[48]

lennard-jones FCC primitive conventional mapping

KPT symmetries

property(k) = property(-k) for all

show how kpts are reduced to first octant using just rotations

show how kpts in first octant are reduced.

B.1.13 Normal Mode Decomposition

harmonic assumption MD is anharmonic

Eigvec mapping

B.1.14 VC-NMD versus Gamma-NMD

B.2 Computability

research.idea = 'string'

B.3 Unsorted

the smartest ppl ion the world shud be using the same shit

B.4 Perspectives

B.4.1 Preparing Journal Articles

The job of the student is to prepare, submit, and (hopefully) publish peer-reviewed journal articles. There are many journals suitable for nanoscale transport topics. Here is one example of the latex files used to create an article used in this work:

This file uses Revtex, which is an article class used by Physical Review, Journal of Applied Physics, and others. The paper can be compiled using:

These can be used as templates

Here is a Carnegie Mellon thesis template:

https://github.com/robsimmons/cmu-thesis

Useful article on structuring large documents

http://web.science.mq.edu.au/ rdale/resources/writingnotes/latexstruct.html

1) Use latex - reccomend Kile editor, gedit works well too. - reccomend zotero to maintain library.bib

1) Time to prepare each paper

reccomendation: student advisor should try and exchange editing a written research document every day, at least every week.

Such a research document could be the running collection of journal articles which turn into the thesis. Maintenance of this document can be achieved with Dropbox or Github. Github offers to advantage of smart version control and internet wiki.

2) Computational cost of each paper

CPU, memory parallel cpu, parallel memory

Trends: small single cpu jobs -¿ large parallel cpu jobs single predictive method -¿ several predictive methods

reccomendation: explore all predictive methods and models possible

B.4.2 Scaling Calculations

combination of increasing hardware, improving software. The improvement of these aspects depends partly on current research.

Have most control over what calculations

Time-scales for data points: 1 sec, 1 min, 1 hour, 1 day, 1 week, 1 month, 1 year number of calculations per PhD: 1E8 , 1E6 , 1E4, 1E3 , 1E2 , 1E1 , 1

1) Run system sizes by doubling. Most calcualtions scale poorly (i.e., $(SYS_S IZE^a lphawithalpha > 1).Pickamaximumsystemsizebasedoncomputatinalresourcesandtimeconstraints.Runallsystemsizesha$

2) Run all trivial (¡ 5 mins) calculations on a given system using all methods possible.

Explore all trivial calculations first. Increase the time-scale and decrease the numner of data-point accordingly.

reccomendation:

B.4.3 Plottable Code

It is important to explore various predictive methods visually. reccomendation: matplotlib provides an enormous number of plotting tools.

Here is a simple example using the python wrapper for lammps with matplotlib to visualize. An MD simuation of LJ argon is visualized. An atom is placed into an unusually high energy position, which initiates melt to the liquid phase.

matplotlib, code version with and without plotting capability.

B.4.4 Scaling into Multi-CPU Dimension

Python w/o shared Memory

Python w/ shared Memory (Parallel Python)

Compiled Code w/ Python Wrapper: Fortran and C++

cython: example LAMMPS python wrapper f2py: simple example. suggest warpper be built for GULP.

B.5 Importance of Open-Source Code

video of python development tree
google+ history with gource
python history with gource
grand-daddy of them all, linux kernel history with gource

It is important that results become more open-source. It's important that our communication becomes open-source. It's important that the entire numerical process be carried out open-source.

B.5.1 Redundancy

There are 3 different codes (shiomi/esfarjani, broido, ankit) for performing the same basic calculations.

For LD, there is GULP, phonopy, SIESTA, etc.

B.5.2 Code Development

took ankit 10 months to re-develop esfarjani code.

code development time can be drastically reduced using pre-existing code. codes written in a modular fashion can be added to easily.

B.5.3 Experiment Pre-dating Simulation

The ideal goal of simulation is to pre-date experiment. This has not been achieved yet. See Fig.

findings for: CNT/Graphene Si Thermoeletric (LUC, alloys, SL, etc) Perovskites PCM

B.5.4   Experiment Pre-dating Simulation

ntpl most cited paper 1-5: maradudin, ladd, dove, ziman,

Bibliography

[1] J. E. Turney. *Predicting phonon properties and thermal conductivity using anharmonic lattice dynamics calculations*. PhD thesis, Carnegie Mellon University, Pittsburgh, PA, 2009.

[2] Yuping He, Davide Donadio, Joo-Hyoung Lee, Jeffrey C. Grossman, and Giulia Galli. Thermal transport in nanoporous silicon: Interplay between disorder at mesoscopic and atomic scales. *ACS Nano*, 5:1839\textbackslashtextbackslashtextbackslashtextbackslashtextbackslash961844, 2011.

[3] D. G. Cahill, W. K. Ford, K. E. Goodson, G. D. Mahan, A. Majumdar, H. J. Maris, R. Merlin, and S. R. Phillpot. Nanoscale thermal transport. *Journal of Applied Physics*, 93:793818, 2003.

[4] A. D. McConnell and K. E. Goodson. Thermal conduction in silicon micro and nanostructures. *Annual Review of Heat Transfer*, 14:129168, 2005.

[5] G. P. Srivastava. *The Physics of Phonons*. Adam Hilger, Bristol, 1990.

[6] D. C. Wallace. *Thermodynamics of Crystals*. Cambridge Univ. Press, Cambridge, UK, 1972.

[7] M. T. Dove. *Introduction to Lattice Dynamics*. Cambridge, Cambridge, 1993.

[8] D. A. Broido, M. Maloney, G. Birner, N. Mingo, and D. Stewart. Intrinsic lattice thermal conductivity of semiconductors from first principles. *Applied Physics Letters*, 91:231922, 2007.

[9] K. Esfarjani, G. Chen, and H. T. Stokes. Heat transport in silicon from first-principles calculations. *Physical Review B*, 84:085204, 2011.

[10] M. Asheghi, Y. K. Leung, S. S. Wong, and K. E. Goodson. Phonon-boundary scattering in thin silicon layers. *Applied Physics Letters*, 71:17981800, 1997.

[11] Alexander Balandin and Kang L. Wang. Significant decrease of the lattice thermal conductivity due to phonon confinement in a free-standing semiconductor quantum well. *Physical Review B*, 58(3):15441549, July 1998.

[12] S.-M. Lee and D. G. Cahill. Heat transport in thin dielectric films. *Journal of Applied Physics*, 81:25902595, 1997.

[13] Zhiting Tian, Keivan Esfarjani, Junichiro Shiomi, Asegun S. Henry, and Gang Chen. On the importance of optical phonons to thermal conductivity in nanostructures. *Applied Physics*

Letters, 99(5):053122, 2011.

[14] A. I. Hochbaum, R. Chen, R. D. Delgado, W. Liang, E. C. Garnett, M. Najarian, A. Majumdar, and P. Yang. Enhanced thermoelectric performance of rough silicon nanowires. *Nature*, 451:163167, 2008.

[15] P. Martin, Z. Aksamija, E. Pop, and U. Ravaioli. Impact of phonon-surface roughness scattering on thermal conductivity of thin si nanowires. *Physical Review Letters*, 102:125503, 2009.

[16] Patrick E. Hopkins, Charles M. Reinke, Mehmet F. Su, Roy H. Olsson, Eric A. Shaner, Zayd C. Leseman, Justin R. Serrano, Leslie M. Phinney, and Ihab El-Kady. Reduction in the thermal conductivity of single crystalline silicon by phononic crystal patterning. *Nano Letters*, 11(1):107112, 2011.

[17] E. S. Landry, M. I. Hussein, and A. J. H. McGaughey. Complex superlattice unit cell designs for reduced thermal conductivity. *Physical Review B*, 77:184302, 2008.

[18] E. S. Landry and A. J. H. McGaughey. Effect of interfacial species mixing on phonon transport in semiconductor superlattices. *Physical Review B*, 79:075316, 2009.

[19] E. S. Landry and A. J. H. McGaughey. Thermal boundary resistance predictions from molecular dynamics simulations and theoretical calculations. *Physical Review B*, 80:165304, 2009.

[20] E. S. Landry and A. J. H. McGaughey. Effect of film thickness on the thermal resistance of confined semiconductor thin films. *Journal of Applied Physics*, 107:013521, 2010.

[21] J. Callaway. Model for lattice thermal conductivity at low temperatures. *Physical Review*, 113:1046, 1959.

[22] M. G. Holland. Analysis of lattice thermal conductivity. *Physical Review*, 132:2461, 1963.

[23] A. J. H. McGaughey, E. S. Landry, D. P. Sellan, and C. H. Amon. Size-dependent model for thin film and nanowire thermal conductivity. *Applied Physics Letters*, 99:131904, 2011.

[24] A. J. C. Ladd, B. Moran, and W. G. Hoover. Lattice thermal conductivity: A comparison of molecular dynamics and anharmonic lattice dynamics. *Physical Review B*, 34:50585064, 1986.

[25] A. J. H. McGaughey and M. Kaviany. Quantitative validation of the boltzmann transport equation phonon thermal conductivity model under the single-mode relaxation time approximation. *Physical Review B*, 69:094303, 2004.

[26] P. K. Schelling, S. R. Phillpot, and P. Keblinski. Comparison of atomic-level simulation methods for computing thermal conductivity. *Physical Review B*, 65:144306, 2002.

[27] D. P. Sellan, E. S. Landry, J. E. Turney, A. J. H. McGaughey, and C. H. Amon. Size effects in molecular dynamics thermal conductivity predictions. *Phys. Rev. B*, 81(21):214305, June 2010.

[28] A. A. Maradudin and A. E. Fein. Scattering of neutrons by an anharmonic crystal. *Physical Review*, 128:25892608, 1962.

[29] A. S. Henry and G. Chen. Spectral phonon transport properties of silicon based on molecu-

lar dynamics simulations and lattice dynamics. *Journal of Computational and Theoretical Nanoscience*, 5:112, 2008.

[30] J. V. Goicochea, M. Madrid, and C. H. Amon. Thermal properties for bulk silicon based on the determination of relaxation times using molecular dynamics. *Journal of Heat Transfer*, 132:012401, 2010.

[31] S. Maruyama. A molecular dynamics simulation of heat conduction of a finite length single-walled carbon nanotube. *Microscale Thermophysical Engineering*, 7:4150, 2003.

[32] Junichiro Shiomi and Shigeo Maruyama. Non-fourier heat conduction in a single-walled carbon nanotube: Classical molecular dynamics simulations. *Phys. Rev. B*, 73:205420, 2006.

[33] J. A. Thomas, J. E. Turney, R. M. Iutzi, C. H. Amon, and A. J. H. McGaughey. Predicting phonon dispersion relations and lifetimes from the spectral energy density. *Physical Review B*, 81:081411(R), 2010.

[34] Zhun-Yong Ong, Eric Pop, and Junichiro Shiomi. Reduction of phonon lifetimes and thermal conductivity of a carbon nanotube on amorphous silica. *Physical Review B*, 84(16):165418, 2011.

[35] Bo Qiu, Hua Bao, Gengqiang Zhang, Yue Wub, and Xiulin Ruan. Molecular dynamics simulations of lattice thermal conductivity and spectral phonon mean free path of PbTe: bulk and nanostructures. *Computational Materials Science*, 53:278\textbackslashtextbackslashtextbackslashtextbackslashtextbackslash96285, 2011.

[36] Junichiro Shiomi, Keivan Esfarjani, and Gang Chen. Thermal conductivity of half-heusler compounds from first-principles calculations. *Physical Review B*, 84(10):125209, 2011.

[37] T. Hori, T. Shiga, S. Maruyama, and J. Shiomi. Mode-dependent phonon transport analysis of silicon crystal by molecular dynamics method. *Tran. of the Jap. Soc. of Mech. Eng.*, 78:328337, 2012.

[38] N. W. Ashcroft and N. D. Mermin. *Solid State Physics*. Saunders, Fort Worth, 1976.

[39] F. H. Stillinger and T. A. Weber. Computer simulation of local order in condensed phases of silicon. *Physical Review B*, 31:52625271, 1985.

[40] W. Rudin. *Real and Complex Analysis*. McGraw-Hill, New York, 1987.

[41] A. J. H. McGaughey, M. I. Hussein, E. S. Landry, M. Kaviany, and G. M. Hulbert. Phonon band structure and thermal transport correlation in a layered diatomic crystal. *Physical Review B*, 74:104304, 2006.

[42] J. M. Ziman. *Electrons and Phonons*. Oxford, New York, 2001.

[43] D. A. McQuarrie. *Statistical Mechanics*. University Science Books, Sausalito, 2000.

[44] J. A. Thomas. *water flow and thermal transport through carbon nanotubes*. PhD thesis, Carnegie Mellon University, Pittsburgh, PA, 2010.

[45] Alan J. H. McGaughey. *Phonon transport in molecular dynamics simulations: Formulation and thermal conductivity prediction*. PhD thesis, University of Michigan, Ann Arbor, MI, 2004.

[46] Steve Plimpton. Fast parallel algorithms for short-range molecular dynamics. *Journal of Computational Physics*, 117(1):1 19, 1995.

[47] J. D. Gale and A. L. Rohl. The general utility lattice program. *Molecular Simulation*, 29:291, 2003.

[48] S. Sinha, P. K. Schelling, S. R. Phillpot, and K. E. Goodsen. Scattering of g-process longitudinal optical phonons at hotspots in silicon. *Journal of Applied Physics*, 97:023702, 2005.

42